

# Environmental Science Nano

Accepted Manuscript



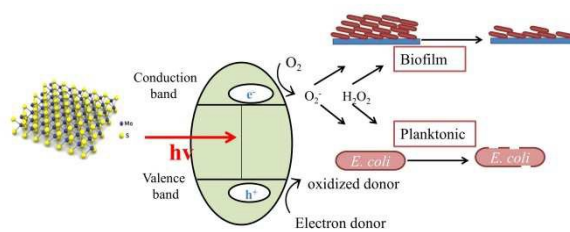
This is an *Accepted Manuscript*, which has been through the Royal Society of Chemistry peer review process and has been accepted for publication.

*Accepted Manuscripts* are published online shortly after acceptance, before technical editing, formatting and proof reading. Using this free service, authors can make their results available to the community, in citable form, before we publish the edited article. We will replace this *Accepted Manuscript* with the edited and formatted *Advance Article* as soon as it is available.

You can find more information about *Accepted Manuscripts* in the [Information for Authors](#).

Please note that technical editing may introduce minor changes to the text and/or graphics, which may alter content. The journal's standard [Terms & Conditions](#) and the [Ethical guidelines](#) still apply. In no event shall the Royal Society of Chemistry be held responsible for any errors or omissions in this *Accepted Manuscript* or any consequences arising from the use of any information it contains.

## Graphical Abstract



EDTA , as an electron donor, used for the first time in the antibacterial study of MoS<sub>2</sub>



## Toxicity of exfoliated-MoS<sub>2</sub> and annealed exfoliated-MoS<sub>2</sub> towards planktonic cells, biofilms, and mammalian cells in the presence of electron donor

Jingjing Fan<sup>a</sup>, Yifei Li<sup>b</sup>, Hang N. Nguyen<sup>a</sup>, Yan Yao<sup>b\*</sup>, Debora F. Rodrigues<sup>a†</sup>

Received 00th January 20xx,  
Accepted 00th January 20xx

DOI: 10.1039/x0xx00000x

www.rsc.org/

We demonstrate for the first time that suspensions of single-layered MoS<sub>2</sub> nanosheets can act as photocatalytic antimicrobial materials under visible light in the presence of ethylenediaminetetraacetic acid (EDTA) as an electron donor. The antimicrobial capacity of exfoliated MoS<sub>2</sub> (Ex-MoS<sub>2</sub>) was found to be 5.7 times higher than that of annealed exfoliated MoS<sub>2</sub> (Ae-MoS<sub>2</sub>) against planktonic cells in the presence of 40 ppm EDTA. This difference in the antimicrobial performance was attributed to the 1T-phase of Ex-MoS<sub>2</sub>, which presents higher electron conductivity than that of Ae-MoS<sub>2</sub>. This higher electron conductivity of Ex-MoS<sub>2</sub> led to increase generation of reactive oxygen species (ROS), as observed by the superoxide anion and hydrogen peroxide production assays under visible light. Additionally, Ex-MoS<sub>2</sub> could also inactivate 65% of mature *E. coli* K12 biofilms without significant cytotoxicity to mammalian fibroblast cells. The suspension of single-layered MoS<sub>2</sub> nanosheets opens up new opportunities for the development of advanced functional nanomaterials for biomedical and environmental applications.

Keywords: Antimicrobial, biofilm, MoS<sub>2</sub>, nanomaterial, planktonic cells

### Nano impacts

This study presents for the first time the mechanisms of antibacterial activity of exfoliated MoS<sub>2</sub> under visible light in the presence of EDTA, as an electron donor. MoS<sub>2</sub> shows great promise as an antibacterial agent against planktonic cells and biofilms without showing adverse cytotoxicity towards mammalian cells. We believe that this study can help and bring a new direction to research on antibacterial applications of nanomaterials under visible light.

### Introduction

Investigation of antimicrobial properties of nanomaterials has recently become a significant topic of discussion due to their large industrial, environmental and biomedical applications.<sup>1-3</sup> For instance, titanium dioxide (TiO<sub>2</sub>) has shown promise in enhancing inactivation of microorganisms on biomedical devices.<sup>4</sup> TiO<sub>2</sub> has also been extensively used in environmental applications for water treatment to eliminate organic compounds and inactivate microorganisms under ultraviolet light. The TiO<sub>2</sub> photocatalytic activity under visible light, however, is almost inexistent due to its large band gap. To address this problem, George and collaborators doped TiO<sub>2</sub> with iron to tune the band gap energy of TiO<sub>2</sub> and enhance its photocatalytic activity under visible light. This procedure, however, led to a nanocomposite material with higher human

toxicity, since further studies of human toxicity with Fe-doped TiO<sub>2</sub> nanorods demonstrated that this nanomaterial could affect liver, heart rate and systolic blood pressure.<sup>5, 6</sup> Thus, it is essential to investigate alternative photocatalysts that are activated under visible light, and are not harmful to humans.

In the present study, we will investigate MoS<sub>2</sub> as a potential photocatalyst under visible light. Besides the photocatalytic activity, this nanomaterial has various unique properties, such as large specific surface area and excellent reactivity.<sup>7</sup> Recent research has briskly investigated several applications of MoS<sub>2</sub>. For instance, this nanomaterial has been shown to be a promising alternative to conventional water treatment by removing dyes from water, via photocatalysis using visible light.<sup>8</sup> MoS<sub>2</sub> also has been extensively investigated for water splitting, organic wastes remediation, and detection of DNA molecules.<sup>9, 10</sup> More recently, researchers have investigated the effects of the MoS<sub>2</sub> nanostructures on their catalytic activity. For instance, Ex-MoS<sub>2</sub> with double gyroid structure (1T-MoS<sub>2</sub> and 2H-MoS<sub>2</sub> mixture) shows much better performance in H<sub>2</sub> evolution compared to bulk MoS<sub>2</sub> (2H-MoS<sub>2</sub>), which is used to synthesize the Ex-MoS<sub>2</sub>.<sup>9</sup> These different nanostructures of MoS<sub>2</sub> have also suggested to have different antibacterial properties, however, so far there are no studies investigating the possible antibacterial mechanisms of these different MoS<sub>2</sub> nanostructures in

<sup>a</sup> Department of Civil and Environmental Engineering, University of Houston, Houston, TX 77204-4003 (USA)

<sup>b</sup> Department of Electrical and Computer Engineering, University of Houston, Houston, TX 77204-4003 (USA)

<sup>†</sup> Corresponding Authors: Dr. Debora F. Rodrigues [dfrigorodrigues@uh.edu](mailto:dfrigorodrigues@uh.edu); Dr. Yan Yao: [yvao4@uh.edu](mailto:yvao4@uh.edu)

† Footnotes relating to the title and/or authors should appear here. Electronic Supplementary Information (ESI) available: [details of any supplementary information available should be included here]. See DOI: 10.1039/x0xx00000x

the presence of electron donors.<sup>11</sup>

In this study, the anti-microbial activity of Ex-MoS<sub>2</sub> and Ae-MoS<sub>2</sub> was investigated using a model bacterial strain, *Escherichia coli* K12<sub>9</sub> in the presence or absence of a sacrificial electron donor and light exposure. In this study the antimicrobial properties of the bulk-MoS<sub>2</sub> was not investigated, since this material is very different from Ex-MoS<sub>2</sub> in many aspects, such as particle size, surface area, phase component and electronic structure. In addition, bulk-MoS<sub>2</sub> cannot be uniformly dispersed into H<sub>2</sub>O, making it difficult to probe the antimicrobial activity under aqueous conditions. The annealed Ex-MoS<sub>2</sub> (Ae-MoS<sub>2</sub>), on the other hand, shares similar properties to Ex-MoS<sub>2</sub> and can be dispersed in H<sub>2</sub>O. Hence, Ae-MoS<sub>2</sub> was used as the control sample. The production of reactive oxygen species (ROS) by these nanomaterials were also evaluated as their possible antimicrobial mechanisms. The production of superoxide anion and hydrogen peroxide by these nanomaterials were evaluated using the 2,3-bis (2-methoxy-4-nitro-5-sulfophenyl)-2H-tetrazolium-5-carboxanilide (XTT) and glutathione (γ-L-glutamyl-L-cysteinylglycine (GSH)) oxidation assays, respectively. The biofilm removal capacity and mammalian cell cytotoxic effects of Ex-MoS<sub>2</sub> were also investigated.

## Experimental

### Synthesis of exfoliated and annealed exfoliated MoS<sub>2</sub>

One gram of bulk MoS<sub>2</sub> (Sigma-Aldrich) was lithiated to form LixMoS<sub>2</sub> by immersing in 6.25 ml n-butyl lithium solution (Sigma-Aldrich, 2.5 M in hexane) and stirred overnight inside a glove box. The LixMoS<sub>2</sub> was filtrated and washed in hexane three times to remove organic residues. The dried LixMoS<sub>2</sub> powder was poured into 100 ml deionized water, sonicated for 1 h, and stirred for another hour to enhance exfoliation. Exfoliated MoS<sub>2</sub> was then centrifuged at 12,000 rpm and washed with deionized water. This process was repeated thrice. After centrifugation, the precipitate was resuspended in water to form stable suspensions of Ex-MoS<sub>2</sub>. The amount of nanomaterial produced was measured by drying the solvent and measuring the weight of the solid content. Annealed exfoliated MoS<sub>2</sub> (Ae-MoS<sub>2</sub>) was prepared by freeze-drying (Labconco, Model 73820) the Ex-MoS<sub>2</sub> suspension and, then by annealing in argon atmosphere at 300 °C for 3 h. The annealed sample was readily dissolved into H<sub>2</sub>O with sonication to form stable suspensions (Ae-MoS<sub>2</sub>). The antibacterial performance assays were conducted immediately after the synthesis.

### SEM, UV-Vis, XPS, XRD and TEM Analyses

Scanning electron microscopy (SEM) images of bulk-, Ex- and Ae-MoS<sub>2</sub> powders were collected with a Gemini LEO 1525 SEM operating at 10 kV. Ultraviolet-visible (UV-Vis) spectrum was measured using the Cary 60 UV-Vis from Agilent Technologies. X-ray photoelectron spectroscopy (XPS) was measured by a Physical Electronics Model 5700 XPS instrument. X-ray diffraction (XRD) was measured using a Rigaku MiniFlex 600 with Cu Kα radiation (λ = 1.5406 Å). Transmission electron microscopy images (TEM) were collected by JEOL 2100F.

For the SEM analysis of the bacteria, aliquots of 1 mL of controls and cells exposed to the Ex-MoS<sub>2</sub> with EDTA were fixed with 2% glutaraldehyde for 1 h and dehydrated by increasing concentrations of ethanol (25, 50, 75, 95, 100% v/v). The pre-treated samples were

mixed with 10 μL of 1,1,1,3,3,3-hexamethyldisilazine (98%, Acros Organics) and then one drop of the solution was placed on a transmission electron microscopy (TEM) grid (CF200-Ni, Cat. No. 71150). After drying the samples overnight at room temperature, specimens were sputter coated with gold (DENTON DESK V HP, Beijing, China). SEM images were acquired in Field-emission SEM (FESEM; LEO 1525, Oberkochen, Germany).

### Bacterial Culture

Before each experiment, a single isolated *E.coli* K12 colony was inoculated into 15 mL tryptic soy broth (TSB) growth medium (Difco Laboratories, Detroit, MI), and incubated overnight at 35 °C. Cells were harvested by centrifugation for 10 min at 4000 rpm and resuspended in phosphate buffer solution (0.01M PBS, pH = 7.4, Fisher Scientific, USA) to an optical density of 0.3 at the wavelength of 600 nm (OD<sub>600</sub>).

### Toxicity of EDTA

This investigation aimed to determine the maximum non-toxic EDTA concentration to be mixed with MoS<sub>2</sub>. The experiment consisted of 20 μL of bacterial suspension in PBS at OD<sub>600</sub> = 0.3 inoculated into a 96-well microtiter plate (Costar 3370, Corning, NY) containing 200 μL of DI water with different concentrations of EDTA ranging from 10 ppm to 150 ppm. A positive control was prepared with 20 μL of bacterial suspension in 200 μL DI water only. Negative control samples were prepared with 200 μL EDTA solution without bacteria. The 96-well microtiter plate was incubated at room temperature for 3 h under visible light. After the incubation period, 20 μL of the bacterial-EDTA suspension was transferred to another 96-well microtiter plate containing 200 μL of TSB. The toxicity was determined by measuring the cell growth at 35°C and 80 rpm with a plate reader spectrophotometer (EL800 universal microplate reader; Bio-Tek Instruments, Inc., Winooske, VT) at 600 nm each hour. Each experiment was performed in triplicate.

### Assessment of MoS<sub>2</sub> nanomaterials toxicity to planktonic cells by plate count method

The antimicrobial assay consisted of different concentrations of Ex-MoS<sub>2</sub> (10 ppm, 50 ppm, 100 ppm and 150 ppm) dispersed in DI water supplemented with 40 ppm of EDTA. A 1 mL volume of bacterial culture at 0.3 OD<sub>600</sub> was added to each concentration and irradiated under two 60 W lamps with constant stirring. To obtain data on the toxic effect of nanomaterials under light exposure, bacterial suspensions were added to the highest pre-determined toxic concentration of nanomaterials. Experiments to simulate dark conditions were performed with plates wrapped in aluminium foil. The number of surviving bacteria was analysed using the drop plate count method after 1 h and 3 h exposure times to the nanomaterials with EDTA.<sup>12</sup> The control samples were prepared in DI water without Ex-MoS<sub>2</sub> and/or EDTA. Colonies were counted and compared to control plates to calculate percentage growth inhibition. All treatments were prepared in triplicate. Identical experiments were also conducted with Ae-MoS<sub>2</sub> and Ex-MoS<sub>2</sub>, to compare the effects of the different nanomaterial structures on toxicity.

### Plate agar assay for assessment of nanomaterial toxicity to biofilms

Circular coverslips with 12 mm in diameter were cleaned with 70% ethanol and deposited at the bottom of 12-well flat-bottom microtiter

plates (Costar 3370, Corning, NY). A volume of 2 mL of bacterial culture at 0.5 OD<sub>600</sub> in TSB was added into the same plate and incubated at 35 °C for 48 h without shaking to achieve mature biofilm on the top of the coverslip. After incubation, the surfaces were gently rinsed with PBS to wash any unattached bacteria to the surface and transferred to another 12 well-plate, which contained different concentration of Ex-MoS<sub>2</sub> (0 ppm, 10 ppm, 50 ppm, 100 ppm and 150 ppm) in DI water supplemented with 40 ppm of EDTA. Controls containing only DI water and DI water with 40 ppm of EDTA without Ex- MoS<sub>2</sub> were also prepared. For the plate agar assay, all the samples were irradiated under two 60 W lamps and incubated for 3 h at 35 °C. After incubation, the coverslips were gently rinsed with PBS and then transferred to TSA plates with the biofilm facing down onto the agar surface. TSA plates were incubated overnight at 35 °C without shaking. The antibacterial activity was determined by measuring the diameter of bacterial growth around the coverslip exposed and not exposed to the nanomaterial. Both control samples, which contained DI water only and DI water with EDTA, were used to evaluate the toxicity. The percent toxicity was calculated from the bacterial growth on the plates based on the following equation:

$$\% \text{ Toxicity} = \frac{(\text{Growth in control} - \text{Growth in sample})}{\text{Growth in control}} \times 100$$

#### Detection of Superoxide Radical Anion (O<sub>2</sub><sup>•-</sup>)

After determining the anti-microbial effects of MoS<sub>2</sub>-EDTA, the mechanism of anti-microbial activity was investigated. To determine the production of superoxide radical anion (O<sub>2</sub><sup>•-</sup>), the XTT (2,3-bis (2,3-bis (2-methoxy-4-nitro-5-sulfophenyl)-2H-tetrazolium-5-carboxanilide, Biotium) assay was performed. The XTT can be reduced by superoxide radical anion (O<sub>2</sub><sup>•-</sup>) to form the water soluble XTT-formazan that has maximum absorption at 470 nm. Briefly, 5 ml of the XTT solution (1mg/ml) and 25 µl of the activation reagent (5 mM phenazine methosulfate (PMS)) were mixed in the dark to produce activated XTT solution. A 2 mL volume of the strongest antibacterial concentrations of Ex-MoS<sub>2</sub> or Ae-MoS<sub>2</sub> were mixed with 1 mL of freshly prepared activated XTT solution. The mixture was incubated under light with constant stirring for 3 h, and then was filtered through a 0.2 µm PTFE membrane filter (Millipore) to remove the nanomaterial. The filtered solution (100 µL) was then placed in a 96-well plate (Corning Inc., USA). The change in absorbance at 470 nm was monitored by the plate reader method (EL800 universal microplate reader; Bio-Tek Instruments, Inc., Winooski, VT). In this assay, 50 ppm and 100 ppm of TiO<sub>2</sub> dispersion exposed to UV light served as positive controls. Negative controls included XTT solution alone and EDTA-XTT mixture. All experiments were done in triplicates and the results were averaged. Standard deviations were calculated based on the triplicate experiments.

#### Thiol Oxidation and Quantification

The Ellman's assay was used to quantify the concentration of thiols in glutathione (GSH).<sup>2</sup> Ex-MoS<sub>2</sub>, Ae-MoS<sub>2</sub>, Ex-MoS<sub>2</sub>-EDTA and Ae-MoS<sub>2</sub>-EDTA solutions were prepared in the following concentrations: 10 ppm, 50 ppm, 100 ppm and 150 ppm. A volume of 225 µL of each solution was added to 225 µL of GSH (0.4 mM in

50 mM bicarbonate buffer) to initiate oxidation. The negative control was the GSH solution only without the nanomaterial, while GSH oxidation by H<sub>2</sub>O<sub>2</sub> (30%) was used as a positive control. All the samples were incubated at room temperature for 2 h at 150 rpm. After incubation, 785 µL of 0.05 M Tris-HCl and 15 µL of DNTB (Ellman's reagent, 5,5'-dithio-bis-(2-nitrobenzoic acid), Sigma-Aldrich) were added into the mixtures to yield a yellow product. All the samples were incubated for another 10 min in the dark, and then filtered through 0.2 µm pore size membrane filters (PTFE Millipore filter, KTGR04FH3). A 250 µL of each filtrate were transferred into a 96-well microtiter plate and the absorbance was measured at 412 nm using Synergy MX Microtiter plate reader (Biotek, U.S.A). The loss of GSH in each sample was calculated by the following formula:

$$\% \text{ GSH loss} = \frac{(\text{absorbance of negative control} - \text{absorbance of sample})}{\text{absorbance of negative sample}} \times 100$$

#### Cytotoxicity using MTS assay

The fibroblast NIH 3T3 cell line was obtained from Professor Ralph B. Arlinghaus (Hubert L. Stringer Chair of Cancer research, MD Anderson Cancer Center, Houston Texas). The cytotoxicity was investigated using CellTiter 96 Aqueous One Solution Cell Proliferation Assay (Promega, U.S.A) with 40 ppm EDTA only, as control, and 40 ppm EDTA with either 100 ppm Ex-MoS<sub>2</sub> or 50 ppm Ae-MoS<sub>2</sub>. The assay contained [3-(4,5-dimethylthiazol-2-yl)-5-(3-carboxymethoxyphenyl)-2-(4-sulfophenyl)-2H-tetrazolium, inner salt (MTS) and an electron coupling reagent, phenazine ethosulfate (PES). More details on the procedure can be found elsewhere.<sup>13</sup>

## Results and discussion

### Synthesis and Characterization of Ex-MoS<sub>2</sub> and Ae-MoS<sub>2</sub>

The MoS<sub>2</sub> samples were synthesized following the procedure described by Eda and collaborators with some modifications (Figure 1(A)).<sup>14</sup> Ex-MoS<sub>2</sub> was produced by exfoliation of lithiated MoS<sub>2</sub> in water to form a quasi-stable suspension of single-layered MoS<sub>2</sub> sheets (see inset of Figure 1(C)). Ae-MoS<sub>2</sub> was re-suspended in water by sonication (see inset of Figure 1(D)). SEM images in Figure 1(B-D) reveal the particle size of the three samples in the form of powders. The starting bulk-MoS<sub>2</sub> materials were aggregates of nanoflakes with diameters of ~1-2 µm. Both Ex-MoS<sub>2</sub> and Ae-MoS<sub>2</sub> samples show large wavy flakes with sizes of ~10-30 µm, completely different from the initial bulk-MoS<sub>2</sub>, indicating a significant structure change during the exfoliation and restacking step. The indirect-direct bandgap transition of MoS<sub>2</sub> after the exfoliation was probed by UV-Vis measurement. For the Ex-MoS<sub>2</sub> dispersions, two peaks can be identified at 623 nm (1.99 eV) and 670 nm (1.85 eV) (Figure S2), which arise from the direct excitonic transitions at the K point of the Brillouin zone, due to the spin-orbital splitting of the valence band.<sup>15, 16</sup> The presence and the absence of peaks at lower energy region of the spectrum are consistent with the results of few- and mono-layered MoS<sub>2</sub>.<sup>15, 17 14</sup> Raman spectroscopy (Figure S3) shows that the wavenumber difference between the E<sub>1</sub>g and A<sub>1</sub>g peaks of Ex-MoS<sub>2</sub> is 2.2 cm<sup>-1</sup> smaller than that of bulk-MoS<sub>2</sub>, which is in agreement with previous reports for few-layered MoS<sub>2</sub> and is attributed to the weakened interlayer interaction.<sup>15, 18</sup>

The XPS analysis of the three samples is shown in Figure 1(E).

Bulk-MoS<sub>2</sub> displayed a Mo 3d<sub>5/2</sub> peak at 229.1 eV and a Mo 3d<sub>3/2</sub> peak at 232.3 eV, manifesting itself as 2H-MoS<sub>2</sub>. After chemical exfoliation, de-convolution of Mo 3d peaks revealed additional peaks at 228.5 eV and 231.65 eV, corresponding to Mo 3d<sub>5/2</sub> and Mo 3d<sub>3/2</sub>, respectively. S2p spectra also presented additional S2p<sub>3/2</sub> and S2p<sub>1/2</sub> peaks at 162.3eV and 161.4 eV respectively, which shifted to lower energy when compared to the peaks of 2H-MoS<sub>2</sub> at 163.1 and 161.9 eV. These new peaks of Mo3d and S2p originated from 1T-MoS<sub>2</sub>, in which the sulfur atoms shifted from the original trigonal prismatic coordination in 2H-MoS<sub>2</sub> to octahedral coordination in 1T-MoS<sub>2</sub> (Figure 1(F)). Therefore, Ex-MoS<sub>2</sub> was determined to be a mixture of 2H and 1T phases. After annealing at 300°C for 3 h, peaks corresponding to 1T-MoS<sub>2</sub> disappeared, indicating that Ae-MoS<sub>2</sub> was mainly 2H-MoS<sub>2</sub>. These results are consistent with the literature report that mild annealing of 1T phase MoS<sub>2</sub> led to gradual transition to 2H phase.<sup>14</sup> XRD results (Figure 1(G)) show that the crystal structures of Ex-MoS<sub>2</sub> and Ae-MoS<sub>2</sub> are similar. Compared with bulk-MoS<sub>2</sub>, a small shift in peak position towards lower angle is observed in both Ex-MoS<sub>2</sub> and Ae-MoS<sub>2</sub>,<sup>25</sup> indicating an increased interlayer distance. Figure S1 shows the high-resolution TEM (HRTEM) images of the cross-sectional view of bulk- and Ex-MoS<sub>2</sub> powders, where the structures along the *c*-axis can be observed. As Figure S1(A) shows, the pristine bulk-MoS<sub>2</sub> has well-ordered layered structure with the interlayer distance of 0.62 nm along *c*-axis. Ex-MoS<sub>2</sub> (Figure S1(B)) has less ordered layered structure with a little larger interlayer distance of 0.64 nm, which agrees well with the broadened and slightly shifted diffraction peak in the XRD spectrum. The weakened crystallinity may be the result

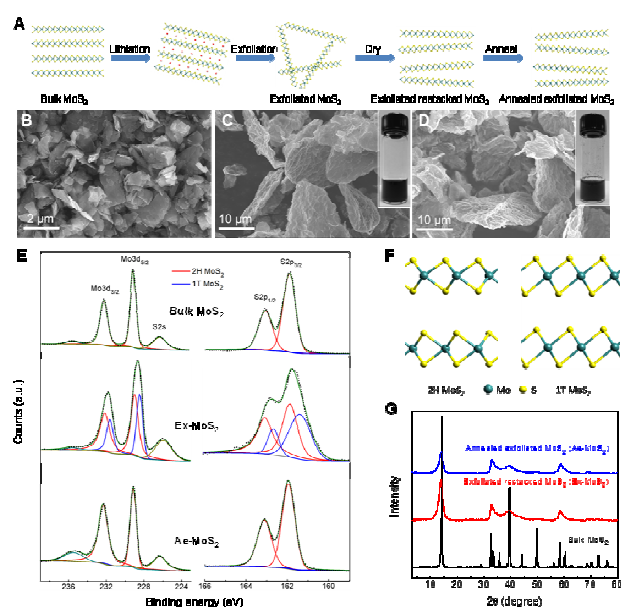


Figure 1. (A) Schematic procedures of three samples used in this study: Bulk MoS<sub>2</sub>, exfoliated MoS<sub>2</sub> (Ex-MoS<sub>2</sub>), dried exfoliated-restacked MoS<sub>2</sub>, and annealed exfoliated MoS<sub>2</sub> (Ae-MoS<sub>2</sub>). SEM images of (B) bulk-MoS<sub>2</sub>, (C) Ex-MoS<sub>2</sub> and (D) Ae-MoS<sub>2</sub> powders. Freshly prepared Ex-MoS<sub>2</sub> suspension and Ae-MoS<sub>2</sub> suspension are shown in the insets of (C) and (D). (E) XPS spectra of Mo 3d, S 2s and S 2p peaks for bulk-MoS<sub>2</sub>, Ex-MoS<sub>2</sub> and Ae-MoS<sub>2</sub>. The Mo 3d and S 2p peaks were de-convoluted into two different phases of MoS<sub>2</sub>: 2H-MoS<sub>2</sub> (red) and 1T-MoS<sub>2</sub> (blue). (F) Atomic structures of 2H-MoS<sub>2</sub> and 1T-MoS<sub>2</sub>. (G) XRD patterns of the three samples.

of the exfoliation-restacking procedure and the increased interlayer spacing may arise from the distortion of MoS<sub>2</sub> layers after restacking.

Ex-MoS<sub>2</sub> and Ae-MoS<sub>2</sub> powders have analogous morphology, similar crystal structures, and only differ in phase compositions. Furthermore, few- and even mono- layers of MoS<sub>2</sub> with direct bandgap structure were confirmed in Ex-MoS<sub>2</sub> dispersions or powders by UV-Vis and Raman spectroscopy. Therefore it would be interesting to compare the antibacterial properties of these two samples.

#### EDTA as a sacrificial donor and its toxicity to bacteria

Previous studies have shown that photocatalytic activity of nanomaterials, such as MoS<sub>2</sub>, can be enhanced in the presence of sacrificial donors.<sup>19</sup> These sacrificial donors donate electrons and keep the photoexcited electrons and holes of nanomaterials separate. In the case of MoS<sub>2</sub>, during water splitting for hydrogen generation, the electron donor transfers electrons to the photocatalyst, here the MoS<sub>2</sub>, leading to a strong reducing conduction band (CB) that can reduce protons to hydrogen molecules.<sup>20, 21</sup> Therefore, we hypothesized that if MoS<sub>2</sub> requires a sacrificial electron donor to more efficiently split water by photocatalysis, it is possible that the inactivation of microorganisms will be enhanced in the presence of a sacrificial donor. Thus, we investigated the effects of the presence of a sacrificial donor, EDTA, on the anti-microbial properties of this nanomaterial.

The rationale for selecting EDTA was that previous studies demonstrated that EDTA was the most effective sacrificial electron donor in water splitting compared to others, such as methanol, ethanol, lactic acid, and formaldehyde.<sup>22</sup> Similarly, other studies also proposed that EDTA could enhance the efficiency of hydrogen generation.<sup>23</sup> Hence, EDTA was selected for further investigation as an electron donor in this study.

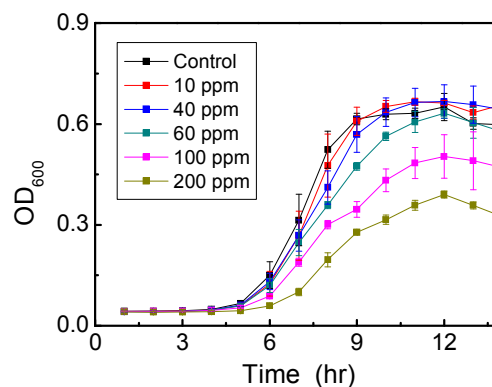


Figure 2. Growth curve of *E. coli* K 12 after exposure to different concentrations of EDTA.

Before performing the experiments with EDTA, as a sacrificial electron donor to MoS<sub>2</sub>, we investigated the toxicity of EDTA to the microbial cells. This investigation aimed to determine the maximum non-toxic EDTA concentration to be used in subsequent experiments with the nanomaterials. The results indicated that concentrations of EDTA below 40 ppm displayed non-toxic effects towards *E. coli* K12 (Figure 2). On the other hand, concentrations higher than 60

ppm were toxic to *E. coli* K12, since longer lag phases and lower optical density values at the stationary phase were observed. Based on our results with the *E. coli* strain K12, the optimum concentration of EDTA to be used with MoS<sub>2</sub> was 40 ppm. Therefore this concentration was used for further investigations to determine the role of the sacrificial electron donor in the antimicrobial properties of MoS<sub>2</sub>.<sup>24, 25</sup>

When comparing MoS<sub>2</sub> in the presence and absence of EDTA under light, the results showed that the presence of EDTA increased the microbial inactivation by more than 50% (Figure 3). This result suggests that EDTA, like in water splitting reaction, plays an important role in the antimicrobial activity of MoS<sub>2</sub>. Additionally, Ex-MoS<sub>2</sub> in the presence of EDTA presented higher antibacterial activity than other well-known nanomaterials. For example, 100 ppm of Ex-MoS<sub>2</sub> presented 36% and 47% higher antibacterial activity than 5000 ppm TiO<sub>2</sub> and SiO<sub>2</sub> under light, respectively.<sup>26</sup> Previous studies have also shown that to achieve similar microbial inactivation to our study, 400 ppm ZnO is necessary, which is three times higher than the concentration used in the present study.<sup>27</sup> Therefore, Ex-MoS<sub>2</sub> can be a potent anti-microbial agent with the advantage of not requiring UV light like TiO<sub>2</sub>.

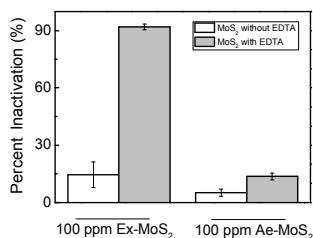


Figure 3. Comparison of *E. coli* K12 inactivation percentages between MoS<sub>2</sub> with EDTA and without EDTA.

#### Effects of contact time, concentration and type of nanomaterials under light and dark conditions on planktonic cells

After determining the highest non-toxic EDTA concentration for *E. coli* K12, the contact time and concentration of the two different types of MoS<sub>2</sub>, namely, Ex-MoS<sub>2</sub> and Ae-MoS<sub>2</sub>, were investigated in the presence of 40 ppm EDTA and under light exposure. The results show that the microbial inactivation is time dependent (Figure 4(A)) since 3 h exposure led to 1.5 to four times greater inactivation than the 1 h exposure for both Ex-MoS<sub>2</sub> and Ae-MoS<sub>2</sub>. Similar toxicity time dependency was observed with other two-dimensional layered materials, like graphene oxide and graphene.<sup>1, 28</sup> This time dependency for microbial inactivation can be explained by the fact that in a shorter exposure time, not all the bacterial cells will have enough time to get into contact or close proximity to the Ex-MoS<sub>2</sub> and Ae-MoS<sub>2</sub> to be fully inactivated. As described later in this study, these nanomaterials under visible light will produce reactive oxygen species (ROS). These ROS are typically produced in close proximity to the nanomaterials. Also, these ROS tend to be unstable over long time periods; therefore the cells need to be relatively close to the nanomaterials that are constantly generating ROS under visible light to be inactivated through ROS. The longer the exposure time, the higher will be the likelihood of a larger number of cells to get in

contact or close proximity to the nanomaterials, which would lead to higher cellular inactivation.

The concentration of Ex-MoS<sub>2</sub> and Ae-MoS<sub>2</sub> also influenced the inactivation of the microorganisms, since increasing concentrations of Ex-MoS<sub>2</sub>, up to 100 ppm, led to higher bacterial inactivation. The maximum bacterial removal was observed at 100 ppm Ex-MoS<sub>2</sub> with 92% inactivation. However, at 150 ppm of Ex-MoS<sub>2</sub>, 48.4% less inactivation than 100 ppm was observed. As mentioned in previously studies, the photocatalytic reaction of MoS<sub>2</sub> may be enhanced with increasing catalyst concentration within a certain range.<sup>29</sup> This phenomenon has been previously described and is called shielding effect. This shield effect occurs when larger amounts of the catalyst is introduced in the reactor creating more active sites for the photocatalytic reaction and increasing the scattering of photons, which in return will decrease the efficiency of the reaction.<sup>30</sup>

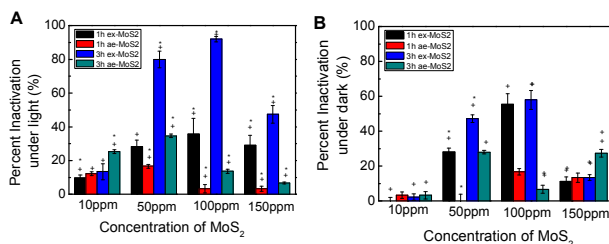


Figure 4 (A) Percent inactivation of *E. coli* exposed to different concentrations of MoS<sub>2</sub>-EDTA under visible light (B) Percent inactivation of *E. coli* exposed to different concentrations of MoS<sub>2</sub>-EDTA under simulated dark conditions. The symbol (\*) corresponds to statistically different results between similar concentrations of MoS<sub>2</sub> under different exposure periods (1h and 3h), while the symbol (+) represents to statistically different results between same exposure period with different concentration of MoS<sub>2</sub>.

Besides the contact time and concentration of the nanomaterials, the type of MoS<sub>2</sub>, also presented different antimicrobial capabilities. For instance, in Figure 4(A), Ex-MoS<sub>2</sub> had 1.7 to 10.7 times higher inactivation capacity than Ae-MoS<sub>2</sub> in the concentration range of 50 to 150 ppm. The lower antimicrobial capacity of Ae-MoS<sub>2</sub> may be explained by its density, the reactivity of the active sites, and poor electrical transport.<sup>31</sup> Similarly, Maitra and collaborators proved that 1T-MoS<sub>2</sub>, major component present in Ex-MoS<sub>2</sub>, is a better catalyst for electrochemical and photochemical hydrogen evolution reactions than Ae-MoS<sub>2</sub>, which only consist of 2H-MoS<sub>2</sub>.<sup>9</sup> Furthermore, the highest cell inactivation performance with Ae-MoS<sub>2</sub> was achieved at 50 ppm, while for Ex-MoS<sub>2</sub> was at 100 ppm. These findings suggest that the different nanomaterial structures have different optimum concentrations for antimicrobial inactivation.

It is worth to note that Ex-MoS<sub>2</sub> showed excellent antibacterial effect under light (Figure 4A). However, to confirm the importance of light in the antimicrobial process of this nanomaterial, antimicrobial experiments were also performed under dark conditions. As shown in Figure 4(B), the highest inactivation percentage of Ex-MoS<sub>2</sub> was found to be 58% after 3 h exposure to 100 ppm, while the maximum inactivation capacity for Ae-MoS<sub>2</sub> was achieved at 50 ppm. A similar inactivation trend was also observed in the experiments conducted under light with increasing concentrations of the nanomaterials (Figure 4(A)), but the light led to higher inactivation values. These results demonstrate that light is an important parameter, which can lead to almost 60% higher inactivation than

dark conditions. Similar findings with TiO<sub>2</sub> were also reported by Daoud and collaborators, which also observed significant bacterial growth reduction after exposure to UV light as opposed to dark conditions.<sup>32</sup> This higher inactivation under light conditions could be explained by higher production of ROS under visible light irradiation of 1T- and 2H-MoS<sub>2</sub> particles.<sup>33</sup>

### Biofilm Removal Capacity of Ex-MoS<sub>2</sub>

Planktonic bacteria in the environment or in engineering processes can form colonies on surfaces to create biofilms.<sup>34</sup> These microbial aggregates, called biofilms, can be 10 to 10000 times less susceptible to antimicrobial compounds than the same organism in suspension, i.e. planktonic phase.<sup>35</sup> These resistant properties of biofilms can lead to antibiotic-resistant infections, clogging of pipes, and contamination of food in industrial settings.<sup>36</sup> Therefore, the investigation of biofilm removal capacity by MoS<sub>2</sub> can be extremely valuable for diverse engineering and biomedical applications.

In the previous section, we determined that the best antibacterial capacity was achieved with Ex-MoS<sub>2</sub> supplemented with 40 ppm of EDTA under light. Thus, the same condition was chosen to perform the biofilm detachment/inactivation investigation. The results (Figure 5) showed that EDTA exhibited negligible toxicity after 3 h exposure. However, the biofilm removal capacity of Ex-MoS<sub>2</sub> increased proportionally to the nanomaterial concentration from 10 to 100 ppm. The maximum biofilm removal (65%) was achieved at 100 ppm by Ex-MoS<sub>2</sub> exposure. When the concentration of Ex-MoS<sub>2</sub> went up to 150 ppm, the biofilm removal decreased to 41.5%.

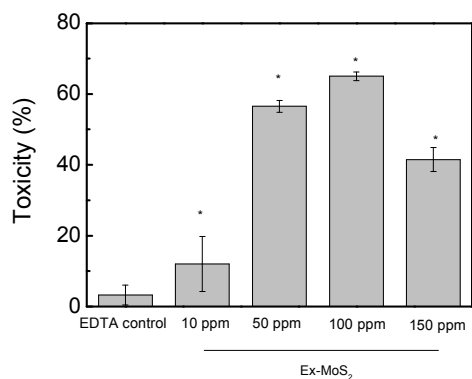


Figure 5. Percent toxicity of different concentrations of Ex-MoS<sub>2</sub> against biofilm. The symbol (\*) correspond to statistically different results between each sample and the control with a 95% confidence interval.

The results of the comparison between planktonic cells and biofilm removal assays after 3 h of Ex-MoS<sub>2</sub> exposure show that the planktonic cells always presented a higher loss of viability than biofilms for all the concentrations investigated. The lower toxicity of Ex-MoS<sub>2</sub> towards biofilm can be explained by the presence of exopolymeric substances (EPS) secreted by biofilms.<sup>35</sup> Several studies have proposed that EPS produced by biofilm can serve as a barrier against nanomaterials, thereby making the nanomaterial less toxic to cells in the biofilm than in planktonic phases.<sup>37, 38</sup> Similar observations have been reported for other antimicrobial chemicals and nanomaterials, like antibiotics, single-walled carbon nanotubes, and graphene oxide.<sup>1, 35</sup> It is also worth to point out that Ex-MoS<sub>2</sub> presented a better performance than other nanomaterials. For instance, the study of Patil and collaborators demonstrated that 250

ppm of ZnO or 100 ppm of Ag/ZnO nanostructures can reduce biofilm growth by 50%.<sup>39</sup> In the case of Ex-MoS<sub>2</sub>, 56.5% reduction of biofilm was obtained with only 50 ppm, which is 2-3 times lower than ZnO and Ag/ZnO. This biofilm reduction in biofilm growth by Ex-MoS<sub>2</sub> can be caused by two potential mechanisms. The first one is that the cells are being inactivated by the ROS produced by the nanomaterials. The second mechanism could be that the reduction in biofilm growth was triggered by photocatalytic degradation or ROS oxidation of quorum sensing molecules involved in biofilm formation. The best performance shown by Ex-MoS<sub>2</sub> compared to the other nanomaterials is probably because this nanomaterial is more efficient in inactivating microorganisms or degrading the quorum sensing molecules.<sup>40</sup>

### Antimicrobial Mechanisms of Ex-MoS<sub>2</sub> and Ae-MoS<sub>2</sub>

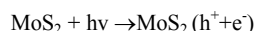
After determining the anti-microbial effects of Ex-MoS<sub>2</sub>-EDTA and Ae-MoS<sub>2</sub>-EDTA on *E. coli*, their anti-microbial activity mechanisms were investigated. Production of ROS is often suggested as a key antibacterial mechanism of several semiconductor and photocatalytic nanomaterials, such as TiO<sub>2</sub> and MoO<sub>3</sub>.<sup>41, 42</sup> Because MoS<sub>2</sub> is also a semiconductor and can perform photocatalytic reactions,<sup>43</sup> we hypothesized that MoS<sub>2</sub> could potentially produce ROS that could be inactivating the microorganisms. Therefore, in this present study we first used the thiol oxidation assay to evaluate the oxidative stress generated by H<sub>2</sub>O<sub>2</sub>.<sup>2</sup> In this assay, EDTA, Ex-MoS<sub>2</sub> and Ae-MoS<sub>2</sub> alone were used as controls. The results show that EDTA (Figure 6(A)) did not generate detectable H<sub>2</sub>O<sub>2</sub>. Ex-MoS<sub>2</sub> and Ae-MoS<sub>2</sub> alone produced some H<sub>2</sub>O<sub>2</sub>, but not as much as the Ex and Ae-MoS<sub>2</sub> with EDTA. In the case of Ae-MoS<sub>2</sub>-EDTA, the highest oxidation capacity (19.8%) towards GSH was observed at 50 ppm. This assay also showed concentration dependency in the range of 50 ppm to 150 ppm (Figure 6(A)). When comparing Ae-MoS<sub>2</sub>-EDTA with Ex-MoS<sub>2</sub>-EDTA, Ae-MoS<sub>2</sub>-EDTA showed less than 35% oxidation capacity than the latter.

Furthermore, increasing concentrations, up to 100 ppm, of Ex-MoS<sub>2</sub> in the presence of EDTA led to higher production of H<sub>2</sub>O<sub>2</sub>. At 150 ppm of Ex-MoS<sub>2</sub>-EDTA, the amount of GSH oxidized was 38.2%. In the absence of EDTA, on the other hand, the GSH oxidation capacity for Ex-MoS<sub>2</sub> were at least 55% less than Ex-MoS<sub>2</sub>-EDTA. The results of the concentration-dependency of oxidation capacity of these nanomaterials were consistent with the antibacterial activity observed in Figure 4 (A) and (B).

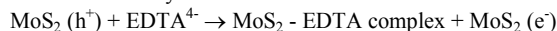
Besides investigating the production of H<sub>2</sub>O<sub>2</sub> by MoS<sub>2</sub>, production of superoxide anion (O<sub>2</sub><sup>-</sup>) was also investigated using the XTT method. In this assay, the Ae-MoS<sub>2</sub> and Ex-MoS<sub>2</sub> concentrations that exhibited the highest antibacterial activity were selected. As shown in Figure 6(B), the negative controls, XTT alone and EDTA-XTT dispersion did not show any increase in absorbance. In the case of Ex-MoS<sub>2</sub>, clear enhancement of absorbance was observed after 120 min incubation, whereas the Ex-MoS<sub>2</sub> did not increase significantly the absorbance. These results indicate that Ex-MoS<sub>2</sub> did not produced superoxide anions, but Ae-MoS<sub>2</sub> produced over time superoxide anions, which would explain not only the different antibacterial activities observed between the Ex-MoS<sub>2</sub> and Ae-MoS<sub>2</sub> presented in Figure 4 (A) and (B), but also the time-dependency of the antibacterial capacity of Ae-MoS<sub>2</sub>.

The mechanisms of production of superoxide ions and hydrogen peroxide by MoS<sub>2</sub> and EDTA are suggested to happen in the

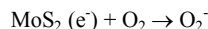
following fashion: the semiconductor photocatalysts are excited by the presence of light to produce electron-hole pairs. Photogenerated electrons migrate to the conduction band, leaving a positive hole in the valence band.



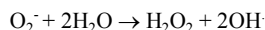
The photoinduced hole can oxidize a donor molecule, which is EDTA in this study. Therefore, EDTA donates the electrons to the VB holes and form MoS<sub>2</sub>-EDTA complex just like the process mentioned in the study of Kim and collaborators.



Oxygen can act as an electron acceptor, and be reduced by the excited electron in the conduction band to form a superoxide ion.



This unstable superoxide can react with water molecules and form hydrogen peroxides, which are responsible for the inactivation of *E. coli*.



The graphical toxicity mechanism of Ex-MoS<sub>2</sub> is also presented in Figure 6(C).

To further confirm the antimicrobial activity of Ex-MoS<sub>2</sub>-EDTA, scanning electron microscope images were taken to determine changes in cell morphology of *E. coli* K12 exposed to Ex-MoS<sub>2</sub>-EDTA. The SEM images (Figure 6(D)) showed that the control cells (not exposed to Ex-MoS<sub>2</sub>-EDTA) were intact and maintained their outer membrane structure. In contrast, in Ex-MoS<sub>2</sub>-EDTA treated cells, instead of normal rod-shaped cells, the cells shrunk and were deformed, indicating cell damage. Previous studies demonstrated that ROS species can increase cell damage and leakage of cell contents, which could also be observed through SEM images like in our study.

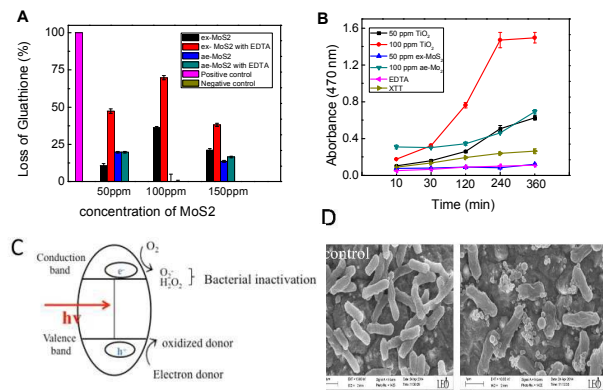


Figure 6. Mechanism of MoS<sub>2</sub> toxicity; (A) Oxidation of glutathione at different concentrations of MoS<sub>2</sub> without EDTA and MoS<sub>2</sub>-EDTA. For positive control H<sub>2</sub>O<sub>2</sub> was used; (B) Production of superoxide radical anion (O<sub>2</sub><sup>-</sup>) by Ex-MoS<sub>2</sub>, Ae-MoS<sub>2</sub>, and EDTA; (C) mechanism diagram for antibacterial activity of MoS<sub>2</sub>; (D) SEM image about *E. coli* before and after exposure to Ex-MoS<sub>2</sub>.

### Cytotoxicity of MoS<sub>2</sub> against NIH 3T3 fibroblast cells

The antibacterial properties of nanomaterials open a window of opportunities for biomedical applications.<sup>48</sup> However, it is critical to evaluate the adverse effects of these nanomaterials to human health for potential applications that will involve human exposure. To investigate the cytotoxic effects of the nanomaterial toward

eukaryotic cells, NIH 3T3 fibroblast cells were exposed for 3 h to MoS<sub>2</sub> concentrations with the highest antimicrobial activity, which was determined to be 50 and 100 ppm for Ae-MoS<sub>2</sub> and Ex-MoS<sub>2</sub>, respectively.

As shown in Figure 7, the cells exposed to Ex-MoS<sub>2</sub> presented no mortality, while the ones exposed to Ae-MoS<sub>2</sub> presented a mortality of 18%. However, ZnO, another widely used nanomaterial, exhibited more than 80% cytotoxicity towards NIH 3T3 fibroblast cells after exposure to 40 ppm.<sup>13</sup> Furthermore, nano-ZnO<sub>2</sub> and nano-TiO<sub>2</sub> also showed 34.4% and 33.7% cytotoxicity, respectively, as reported in a previous study.<sup>49</sup> Therefore, the very low cytotoxicity observed for Ex-MoS<sub>2</sub> makes it a very promising material for applications involving human exposure.

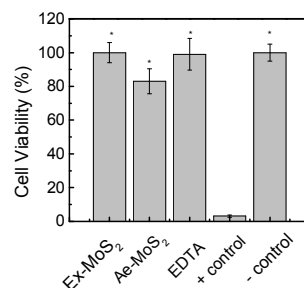


Figure 7. Percent cytotoxicity of NIH 3T3 fibroblast cells after 3 h of exposure to 100 ppm Ex-MoS<sub>2</sub>, 50 ppm Ae-MoS<sub>2</sub>, and 40 ppm of EDTA. Untreated cells were used as negative controls, and PBS with 0.02% benzalkonium chloride were added to the wells containing cells and used as positive controls. The symbol (\*) correspond to statistically different results between each sample and the positive control with a 95% confidence interval

### Conclusions

The antibacterial activity of Ex-MoS<sub>2</sub> and Ae-MoS<sub>2</sub> in the presence or absence of light and sacrificial electron donor was evaluated. Ex-MoS<sub>2</sub> demonstrated higher antibacterial capacity than Ae-MoS<sub>2</sub>. The addition of electron donors and light source increased the antibacterial activity by more than 50%. The antibacterial activity of MoS<sub>2</sub> may be attributed to oxidative stress coming from superoxide radical anion (O<sub>2</sub><sup>-</sup>) and hydrogen peroxide (H<sub>2</sub>O<sub>2</sub>). The higher antibacterial capacity of Ex-MoS<sub>2</sub> than Ae-MoS<sub>2</sub> may be mostly due to a higher ratio of metallic 1T-phase. Most importantly, compared with the most commonly used photocatalyst, i.e. TiO<sub>2</sub>; Ex-MoS<sub>2</sub> was demonstrated to have higher antibacterial effects in the presence of an electron donor with the advantage of activation under visible light. Additionally, we confirmed that Ex-MoS<sub>2</sub> was not toxic to fibroblast cells. Nanomaterials with efficient antibacterial properties and that are non-toxic to humans have an enormous potential for industrial, biomedical, and water treatment applications. Thus, the potential of this nanomaterial for uses in biomedical applications is enormous, because of its antibacterial properties and low toxic effects to mammalian cells.

### Acknowledgements

We would like to thanks Dr. Felipe Ibanez for assisting with the agar plate count method and Professor Ralph B. Arlinghaus for giving us the mammalian cells for this investigation. Y. Yao acknowledge the

funding support from the Office of Naval Research Young Investigator Award (ONR N00014-13-1-0543) for the synthesis and characterization of MoS<sub>2</sub> samples.

## Reference

- I. E. Mejias Carpio, C. M. Santos, X. Wei and D. F. Rodrigues, *Nanoscale*, 2012, 4, 4746-4756.
- S. Liu, T. H. Zeng, M. Hofmann, E. Burcombe, J. Wei, R. Jiang, J. Kong and Y. Chen, *ACS nano*, 2011, 5, 6971-6980.
- M. N. Chong, B. Jin, C. W. Chow and C. Saint, *Water research*, 2010, 44, 2997-3027.
- C. Srinivasan and N. Somasundaram, *Curr Sci India*, 2003, 85, 1431-1438.
- S. George, S. Pokhrel, Z. Ji, B. L. Henderson, T. Xia, L. Li, J. I. Zink, A. E. Nel and L. Madler, *J Am Chem Soc*, 2011, 133, 11270-11278.
- A. Nemmar, K. Melghit, S. Al-Salam, S. Zia, S. Dhanasekaran, S. Attoub, I. Al-Amri and B. H. Ali, *Toxicology*, 2011, 279, 167-175.
- X. Zong, Y. Na, F. Wen, G. Ma, J. Yang, D. Wang, Y. Ma, M. Wang, L. Sun and C. Li, *Chemical communications*, 2009, DOI: 10.1039/b907307h, 4536-4538.
- T. R. Thurston and J. P. Wilcoxon, *The Journal of Physical Chemistry B*, 1998, 103, 11-17.
- U. Maitra, U. Gupta, M. De, R. Datta, A. Govindaraj and C. N. Rao, *Angewandte Chemie*, 2013, 52, 13057-13061.
- C. F. Zhu, Z. Y. Zeng, H. Li, F. Li, C. H. Fan and H. Zhang, *Journal of the American Chemical Society*, 2013, 135, 5998-6001.
- N. Qureshi, R. Patil, M. Shinde, G. Umarji, V. Causin, W. Gade, U. Mulik, A. Bhalerao and D. Amalnerkar, *Appl Nanosci*, 2015, 5, 331-341.
- H. J. Hoben and P. Somasegaran, *Applied and environmental microbiology*, 1982, 44, 1246-1247.
- T. O. Okyay, R. K. Bala, H. N. Nguyen, R. Atalay, Y. Bayam and D. F. Rodrigues, *RSC Advances*, 2015, 5, 2568-2575.
- G. Eda, H. Yamaguchi, D. Voiry, T. Fujita, M. Chen and M. Chhowalla, *Nano Letters*, 2011, 11, 5111-5116.
- A. Splendiani, L. Sun, Y. Zhang, T. Li, J. Kim, C.-Y. Chim, G. Galli and F. Wang, *Nano Letters*, 2010, 10, 1271-1275.
- O. Y. Posudievsky, O. A. Khazieieva, V. V. Cherepanov, G. I. Dovbeshko, A. G. Shkavro, V. G. Koshechko and V. D. Pokhodenko, *Journal of Materials Chemistry C*, 2013, 1, 6411-6415.
- K. F. Mak, C. Lee, J. Hone, J. Shan and T. F. Heinz, *Physical review letters*, 2010, 105, 136805.
- H. Li, Z. Yin, Q. He, H. Li, X. Huang, G. Lu, D. W. H. Fam, A. I<sub>400</sub> Y. Tok, Q. Zhang and H. Zhang, *Small*, 2012, 8, 63-67.
- A. Galińska and J. Walendziewski, *Energy & Fuels*, 2005, 19, 1143-1147.
- M. R. Hoffmann, S. T. Martin, W. Choi and D. W. Bahnemann, *Chemical Reviews*, 1995, 95, 69-96.
- A. Kudo and Y. Miseki, *Chemical Society Reviews*, 2009, 38, 253-278.
- U. Pal, S. Ghosh and D. Chatterjee, *Transition Met Chem*, 2012, 37, 93-96.
- M. Ni, M. K. H. Leung, D. Y. C. Leung and K. Sumathy, *Renewable and Sustainable Energy Reviews*, 2007, 11, 401-425.
- B. M. Rathgeber, P. McCarron and K. L. Budgell, *Poultry Science*, 2013, 92, 2457-2462.
- A. D. Satroudinov, E. G. Dedyukhina, T. I. Chistyakova, I. G. Minkevich, V. K. Eroshin and T. Egli, *Microbiology*, 2003, 72, 8-11.
- L. K. Adams, D. Y. Lyon and P. J. Alvarez, *Water research*, 2006, 40, 3527-3532.
- N. Padmavathy and R. Vijayaraghavan, *Sci Technol Adv Mat*, 2008, 9.
- X. Yang, J. Li, T. Liang, C. Ma, Y. Zhang, H. Chen, N. Hanagata, H.-X. Su and M. Xu, *Nanoscale*, 2014, DOI: 10.1039/C4NR01965B.
- D. Pei and J. Luan, *International Journal of Photoenergy*, 2012, 2012, 13.
- P. H. Chen, C. Y. Chen and C. H. Jenq, *Water Supply*, 1995, 13, 29-34.
- M. A. Lukowski, A. S. Daniel, F. Meng, A. Forticaux, L. Li and S. Jin, *Journal of the American Chemical Society*, 2013, 135, 10274-10277.
- W. A. Daoud, J. H. Xin and Y.-H. Zhang, *Surface Science*, 2005, 599, 69-75.
- W. Kangwansupamonkon, V. Lauruengtana, S. Surasmo and U. Ruktanonchai, *Nanomedicine : nanotechnology, biology, and medicine*, 2009, 5, 240-249.
- D. G. Davies, M. R. Parsek, J. P. Pearson, B. H. Iglewski, J. W. Costerton and E. P. Greenberg, *Science*, 1998, 280, 295-298.
- D. F. Rodrigues and M. Elimelech, *Environmental Science & Technology*, 2010, 44, 4583-4589.
- M. A. Schembri, K. Kjaergaard and P. Klemm, *Molecular microbiology*, 2003, 48, 253-267.
- I. W. Sutherland, *Microbiology*, 2001, 147, 3-9.
- M. Starkey, K. A. Gray, S. I. Chang and M. R. Parsek, *Microbial biofilms. ASM Press, Washington, DC*, 2004, 174-191.
- S. Patil, R. Patil, S. Kale, M. Tamboli, J. Ambekar, W. Gade, S. Kolekar and B. Kale, *J Nanopart Res*, 2014, 16, 1-11.
- S. Gurunathan, J. Han, D.-N. Kwon and J.-H. Kim, *Nanoscale Res Lett*, 2014, 9, 1-17.
- K. Krishnamoorthy, M. Premanathan, M. Veerapandian and S. J. Kim, *Nanotechnology*, 2014, 25, 315101.
- S. Liu, T. H. Zeng, M. Hofmann, E. Burcombe, J. Wei, R. Jiang, J. Kong and Y. Chen, *ACS Nano*, 2011, 5, 6971-6980.
- K. Sunada, Y. Kikuchi, K. Hashimoto and A. Fujishima, *Environmental Science & Technology*, 1998, 32, 726-728.
- G. Kim and W. Choi, *Applied Catalysis B: Environmental*, 2010, 100, 77-83.
- I. Sondi and B. Salopek-Sondi, *J Colloid Interf Sci*, 2004, 275, 177-182.
- S. Kang, M. Pinault, L. D. Pfefferle and M. Elimelech, *Langmuir : the ACS journal of surfaces and colloids*, 2007, 23, 8670-8673.
- S. C. Smith and D. F. Rodrigues, *Carbon*, DOI: <http://dx.doi.org/10.1016/j.carbon.2015.04.043>.
- F. Ahmed, C. M. Santos, R. A. M. V. Vergara, M. C. R. Tria, R. Advincula and D. F. Rodrigues, *Environmental Science & Technology*, 2011, 46, 1804-1810.

49. G. Karunakaran, R. Suriyaprabha, P. Manivasakan, R. Yuvakkumar, V. Rajendran and N. Kannan, *Ecotoxicology and environmental safety*, 2013, 93, 191-197.

ARTICLE

---

Environmental Science: Nano Accepted Manuscript